Applied Physics Letters ARTICLE pubs.aip.org/aip/apl

Strain effects on Auger–Meitner recombination in silicon

Cite as: Appl. Phys. Lett. **123**, 262105 (2023); doi: 10.1063/5.0176950
Submitted: 18 September 2023 · Accepted: 13 December 2023 ·
Published Online: 27 December 2023

Kyle Bushick[1,2] and Emmanouil Kioupakis[1,a)]

AFFILIATIONS

[1]Department of Materials Science and Engineering, University of Michigan, Ann Arbor, Michigan 48109, USA
[2]Materials Science Division, Lawrence Livermore National Laboratory, Livermore, California 94550, USA

[a)]Author to whom correspondence should be addressed: kioup@umich.edu

ABSTRACT

We study the effects of compressive and tensile biaxial strain on direct and phonon-assisted Auger–Meitner recombination (AMR) in silicon using first-principles calculations. We find that the application of strain has a non-trivial effect on the AMR rate. For most AMR processes, the application of strain increases the AMR rate. However, the recombination rate for the AMR process involving two holes and one electron is suppressed by 38% under tensile strain. We further analyze the specific phonon contributions that mediate the phonon-assisted AMR mechanism, demonstrating the increased anisotropy under strain. Our results indicate that the application of tensile strain increases the lifetime of minority electron carriers in *p*-type silicon and can be leveraged to improve the efficiency of silicon devices.

Auger–Meitner recombination (AMR) is a non-radiative recombination process intrinsic to semiconductor materials that involves three carriers. In AMR, an electron–hole pair recombines across the bandgap, transferring the excess energy through the Coulomb interaction to a third carrier, either an electron or a hole, which is itself promoted to a higher energy state. If the third carrier is an electron, we denote this as the electron–electron–hole (*eeh*) process, while if the third carrier is a hole, we denote this as the hole–hole–electron (*hhe*) process. Furthermore, AMR can occur either in a direct manner, where energy and momentum are strictly conserved between the participating carriers, or in an indirect (phonon-assisted) manner, where one of the carriers can absorb or emit a phonon, relaxing the momentum conservation constraints and enabling excitations to a broader range of high-energy states. Historically, this process has been known as Auger recombination, but the renaming to Auger–Meitner aims to recognize the contributions of Lise Meitner in the discovery of the effect.[1] In silicon, AMR acts as a loss mechanism, limiting the efficiency of numerous devices including solar cells,[2–5] transistors,[6,7] and diodes.[6,8]

In many functional applications, applying a small amount of strain is a technique that can be used to tune the material properties and improve device performance.[9–11] This is the case both for silicon and for other materials.[12–18] However, there is little work in the literature on the effects of strain on AMR in silicon, a deficiency we aim to address in our work. Ultimately, it is of interest to modulate the AMR rate in devices—either to mitigate its effects as a non-radiative loss mechanism[19–21] or to intentionally increase the generation of hot carriers.[22–24] In the case of silicon devices, we are mostly interested in the former. Considering AMR is an intrinsic material property that is independent of defects present in the material, engineering solutions that aim to improve the chemical purity or structural quality are not viable methods to control the AMR rate. However, affecting the underlying electronic structure is a viable option for controlling the AMR rate. As has been shown in previous work on InGaAs/InGaAsP quantum well lasers, the application of compressive strain is a viable strategy to suppress AMR by affecting the valence band curvature and, therefore, the availability of holes that satisfy both momentum and energy conservation constraints.[25] While this specific AMR-suppression mechanism does not translate to bulk silicon—for which direct *hhe* AMR is negligible compared to other AMR pathways[26]—there may be other modifications to the band structure that affect the AMR rate. Specifically, the application of biaxial strain allows one to alter the valley and band degeneracy of electrons and holes. In the case of the electrons in silicon, the sixfold valley degeneracy is split, with the valleys along the direction of crystal compression (four in-plane for compressive and two out-of-plane for tensile biaxial strain) lowering in energy. For holes, the valence band maximum is at the Γ-point, so there is no valley degeneracy; however, the application of strain reduces the band degeneracy with one and two band(s) lowering in energy under the application of compressive and tensile biaxial strain, respectively. These effects are illustrated in Fig. 1 (we cover the strain

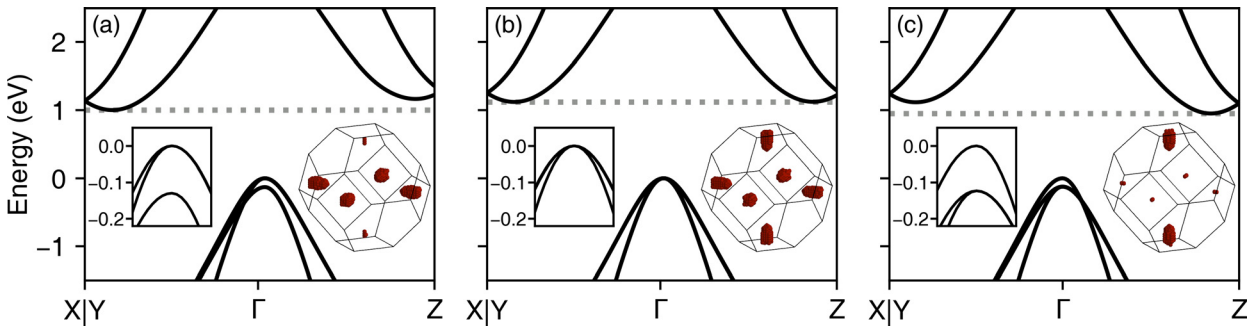

FIG. 1. Effects of biaxial strain on the band structure of silicon. 1% compressive (a), unstrained (b), and 1% tensile (c) conditions are shown. The left inset shows a zoomed view of the valence band edges, while the right inset shows the relative occupation of the conduction band valleys in the first Brillouin zone. The gray dotted lines are guides to the eye to show the conduction band energy splitting.

effects on the phonon dispersion in the supplementary material). In the context of AMR, these alterations to the band structure lead to non-trivial impacts on the recombination rates, emphasizing the need for first-principles characterization techniques.

In this Letter, we apply our first-principles methodology to characterize the effects of compressive and tensile biaxial strain on both the direct and phonon-assisted AMR rate in crystalline silicon. We show that the AMR coefficient increases for both *eeh* and *hhe* AMR under compressive strain as well as *eeh* AMR under tensile strain. Notably, we find a ∼40% reduction in the *hhe* AMR coefficient under tensile strain. We also analyze the contributions of different phonon modes to the phonon-assisted AMR process under various strain conditions. Finally, we discuss how our findings can inform the application of strain to improve silicon device performance.

Our calculation methodology uses eigenvalues, wave functions, and electron–phonon coupling matrix elements generated by density functional theory (DFT) and density functional perturbation theory (DFPT) calculations, which we obtain using the `Quantum ESPRESSO` code[27–29] within the local density approximation (LDA) for the exchange-correlation functional.[30,31] We use a Troullier-Martins[32] norm-conserving pseudo-potential throughout our calculations. We use a relaxed lattice parameter of $a = 5.379$ Å for the unstrained structure. To obtain the biaxially strained structures, we adjust the in-plane lattice constants (X and Y) by $\mp 1\%$ and allow the out-of-plane Z direction to relax. This gives us an out-of-plane lattice parameter of 5.420 Å for the compressive biaxial strain condition and 5.337 Å for the tensile biaxial strain condition.

We chose to study this magnitude of strain because it is readily achievable in real systems and leads to sizable valley (>170 meV) and band (>125 meV) energy splitting for the electrons and holes, respectively [Figs. 1(a) and 1(c)]. It is important to achieve splitting much larger than k_BT (∼26 meV) to ensure that carriers selectively occupy the lower-energy states, since otherwise the AMR rates would be approximately equal to those of unstrained Si. While we expect a smooth transition from the unstrained to the 1% strain AMR values as energy splitting goes from zero to $>k_BT$, once a substantial polarization of the state occupancies is achieved, further increases to the strain are not expected to yield large variations in the AMR coefficients. Since the spin–orbit splitting is only ∼45 meV in silicon,[33,34] the band structure splitting effects are dominated by strain. Furthermore, the work by Zacharias, Scheffler, and Carbogno on unstrained silicon has shown that the electron–phonon renormalization of the bandgap is approximately 60 meV at 0 K and less than 100 meV at 300 K.[35] The explicit inclusion of these effects is beyond the scope of our work, but we expect the electron–phonon renormalization to be similar for the energy-split states, and, thus, it should only have a minor effect on the AMR coefficients in strained silicon. The 1% strain value is, therefore, sufficiently high enough to achieve the full effects of strain on the AMR coefficients while simultaneously being low enough to realize experimentally.

We calculated the LDA eigenvalues on an $8 \times 8 \times 8$ Brillouin-zone sampling grid and interpolated them to fine grids using the maximally localized Wannier-function method[36] and the `Wannier90` code.[37] While we performed G_0W_0 (GW) calculations to obtain quasiparticle corrections to the LDA eigenenergies for all three structures, we found that in all cases, the GW corrections were effectively rigid shifts to the band gaps (Fig. S2). To avoid the added complexity of performing Wannier-function interpolation on the GW quasiparticle energies to arbitrary **k**-points, we opted to rigidly shift the band gaps to 1.00 eV for the compressed system, 1.12 eV for the unstrained system, and 0.95 eV for the tensile system. These values were chosen because they are consistent with the experimental value for unstrained silicon,[38] the LDA bandgap differences between the strained and unstrained structures as well as with experimental bandgap values for strained silicon reported in the literature.[39] To calculate the AMR coefficients, we used the same converged Brillouin-zone sampling grids of $50 \times 50 \times 50$ and δ-function broadenings of 0.1–0.2 eV discussed in our previous work.[26] We use a temperature of 300 K and free-carrier concentration of 10^{18} cm^{-3} throughout our calculations. Under these conditions, Coulomb-enhancement effects to the AMR rate that arise from many-body interactions are weak and can be safely ignored.[26,40]

To perform our AMR calculations for strained silicon, we applied first- and second-order time dependent perturbation theory in the Fermi's golden rule framework, as outlined in our previous work on unstrained silicon.[26] From these calculations, we obtain the AMR rate, $R = \frac{dN}{dt} = CVn^3$, where the carrier density $n = \frac{N}{V}$ denotes the number of free carriers N per volume V and C is the AMR coefficient. For direct AMR, we make no assumptions about the Brillouin-zone distribution of the free carriers as a function of strain conditions, and there are, therefore, no differences in our approach compared to those discussed in Refs. 26 and 41. As we show in the insets of Figs. 1 and S3 in greater detail, the majority (>97%) of electrons occupy the lower-

energy conduction band valley (while the holes are primarily restricted to the top valence band). Given this information and the assumptions needed for the computational tractability of the phonon-assisted calculations (that the periodic part of the wave functions of carriers are approximately equal to those of the nearest band extremum), we restrict $N^{\mathbb{C}}_{valley} = 4$ for compressive strain and $N^{\mathbb{C}}_{valley} = 2$ for tensile strain. Similarly, we restrict $N^{\mathbb{V}}_{band} = 2$ for compressive strain and $N^{\mathbb{V}}_{band} = 1$ for tensile strain. This captures the effects of strain on the band structure while keeping the calculation computationally feasible. We do not include the effects of spin–orbit splitting in our calculations, as the energy splitting due to strain is approximately 3× stronger, as we discuss earlier.

Using our computational approach outlined earlier, we report the *eeh* and *hhe* AMR rates across the three strain conditions (compressive, unstrained, and tensile) in Fig. 2 and Table I. We break down the total AMR coefficient in terms of the direct and phonon-assisted contributions. As expected, our results for the unstrained system are consistent with past work, both theoretical and experimental.[26,42–44] The similarity between our unstrained values and past results indicates the validity of using the LDA eigenvalues with a rigid shift in place of the GW quasiparticle energies. Under the application of compressive strain, we find $C_{eeh,dir}$ increases by 56%, $C_{eeh,pa}$ increases by 77%, $C_{hhe,dir}$ increases by 51%, and $C_{hhe,pa}$ increases by 13%. In the case of tensile strain, we find $C_{eeh,dir}$ increases by 119%, $C_{eeh,pa}$ increases by 139%, $C_{hhe,dir}$ decreases by 75%, and $C_{hhe,pa}$ decreases by 38%. Under all strain conditions, the direct *hhe* AMR process is effectively forbidden due to momentum conservation, and so *hhe* AMR is entirely accounted for by the phonon-assisted process. As we show, applying strain generally increases the AMR rate, with the exception of *hhe* under tensile strain. This is largely consistent with previous work on strained germanium, which found that both direct and phonon-assisted AMR increased under strain, though these results coincide with an indirect-to-direct bandgap transition in germanium, which we attribute as the cause for the differing behavior.[45]

Two competing effects alter the AMR rate due to the symmetry and degeneracy breaking induced by strain: (1) selective occupation of bands with reweighted matrix elements and (2) a reduced number of recombination channels. The interplay between these two effects is clearly seen in Fig. 3, where *f*-type (*eeh*) AMR is eliminated in the tensile condition, but the strength of the *g*-type and intravalley processes is significantly enhanced. Note that since both holes for *hhe* AMR occupy the same Γ valley, there is no distinction between their initial valley arrangement. Further discussion of the valley analysis is included in the supplementary material. Since we expect a decrease in AMR due to the reduction of recombination channels but consistently observe an increase in the AMR rates, we conclude that the selective band occupancy dominates the effects of strain on AMR. However, the non-trivial effects on the AMR coefficient that result from the competition and interplay between these strain-induced mechanisms highlight the need for the first-principles approach employed in this investigation.

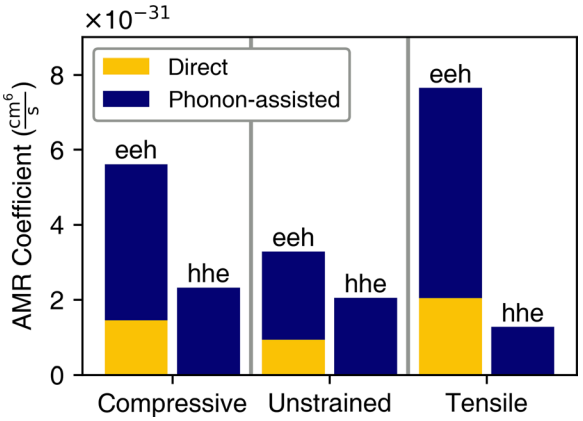

FIG. 2. Effects of strain on the *eeh* and *hhe* AMR coefficients in silicon. The contributions from the direct process are shown in gold, while the contributions from the phonon-assisted process are shown in blue. Direct *hhe* is forbidden by momentum conservation under all strain conditions, and only the *hhe* process is reduced by the application of tensile strain.

TABLE I. Calculated AMR coefficients under different strain conditions. All values are in units of $\times 10^{-31}$ cm^6 s^{-1}.

Strain condition	$C_{eeh,dir}$	$C_{eeh,pa}$	$C_{hhe,dir}$	$C_{hhe,pa}$
−1% strain	1.45	4.17	0.000 029 3	2.32
No strain	0.932	2.35	0.000 019 4	2.05
+1% strain	2.04	5.62	0.000 004 89	1.27

An additional benefit of leveraging first-principles calculations is the ability to obtain insights into the underlying mechanisms of AMR. Figure 4 details the contributions of different phonons to the overall phonon-assisted AMR process, expressed in terms of distributions over phonon energy and phonon momentum. The integration of these distributions yields the total AMR coefficient. The three-dimensional momentum distribution is shown in Fig. S4. We find that the distribution over phonon modes is reweighted through the application of strain. These effects are most clearly seen in the *eeh* process under tensile strain but are present under all conditions. Of particular note for the phonon-assisted *eeh* AMR under tensile strain is the emergence of a third peak at a phonon energy of 45 meV as well as a prominent renormalization at the phonon wave vector magnitude of 0.55 a.u.$^{-1}$, which corresponds to phonons with $\mathbf{q} \approx \Delta_Z$, i.e., the momentum of the low-energy out-of-plane electron valley. The magnitude of this phonon mode contribution also indicates a larger matrix element for this transition under tensile strain. The effects of compressive strain on the distribution are less pronounced, which is intuitive, given that the band structure more closely resembles that of the unstrained system, and no recombination pathways are forbidden, unlike in the tensile case. We also analyze the excited electron distribution in the supplementary material (Fig. S5), highlighting the anisotropy of the direct *eeh* AMR process.

Our results provide insights not only into the microscopic mechanisms governing AMR in strained silicon but also into the potential application of strain to improve silicon device performance. Indeed, silicon devices are incredibly varied and technologically critical. They encompass diverse electronic and optoelectronic applications from solar cells to transistors, playing a critical role in both our energy and computing infrastructure. In many of these applications, AMR is known to act as a loss mechanism, which reduces their overall efficiency and performance. This is notable in solar cells, transistors, thyristors, and *p*–*n* junctions more generally.[2–7,46] Unfortunately, it is

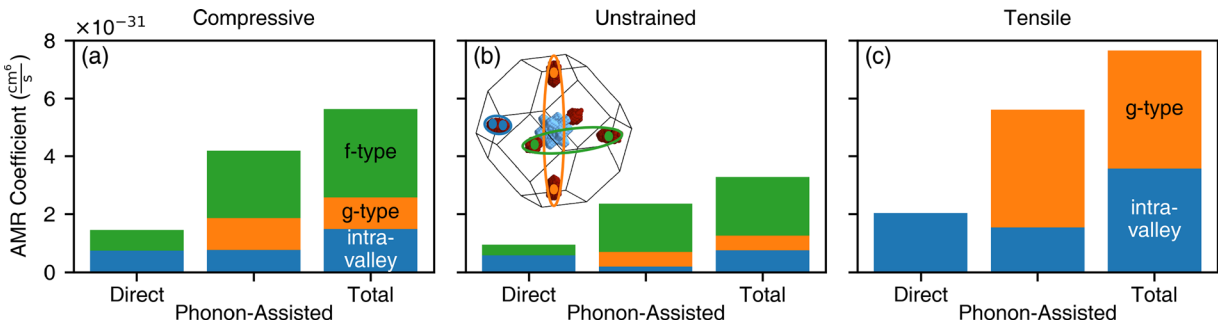

FIG. 3. Breakdown of *eeh* AMR for direct and phonon-assisted processes in strained silicon. The broken valley degeneracy affects the effective carrier concentration and available scattering pathways for the low-energy electrons. The most notable effect is the elimination of *f*-type AMR under tensile strain. The inset plot in (b) serves as a visual key for the different recombination types, with the colors matching the bar colors (intravalley = blue, *g*-type = orange, and *f*-type = green).

challenging to adjust one intrinsic material property (e.g., bandgap, mobility, or carrier lifetime) by strain in isolation. While we focus on the effects of strain on AMR in this Letter, we note the fact that both compressive and tensile biaxial strain decrease the bandgap of silicon.

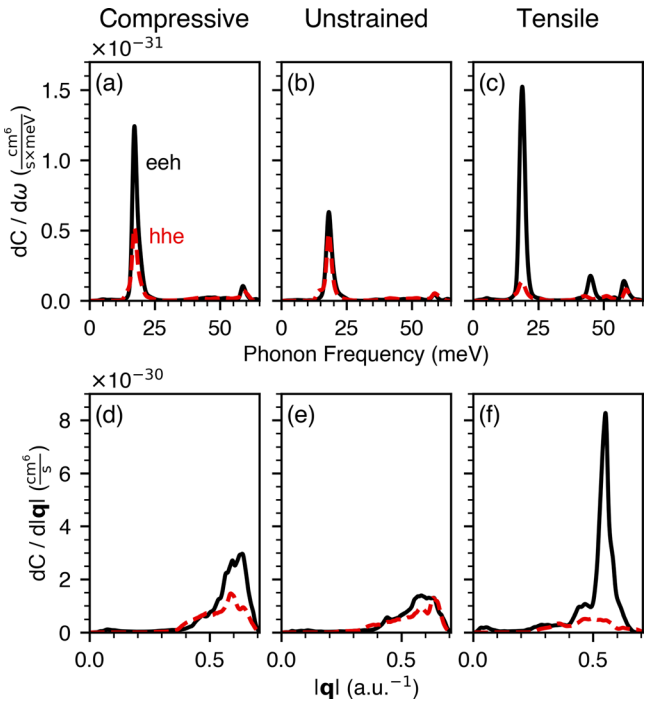

FIG. 4. Phonon decomposition of the phonon-assisted *eeh* (solid black) and *hhe* (dashed red) AMR coefficients. (a)–(c) The dependence of the AMR coefficient on the phonon frequency for the compressive, unstrained, and tensile systems. The distribution is mostly consistent across the strain conditions, with the *hhe* process becoming relatively weaker compared to the *eeh* process under strain. The *eeh* process under tensile strain shows the emergence of a new contribution by phonons at 45 meV. (d)–(f) The AMR distribution as a function of phonon wave-vector magnitude across the three strain conditions. The qualitative observations are consistent with the energy decomposition, though the tensile *eeh* process also shows a prominent peak corresponding to $\mathbf{q} \approx \Delta_Z$.

Other works have also discussed the effects of strain on the carrier mobility, which is a property of great importance to many devices.[47] Specifically, applying strain on the order of $\mp 1\%$ leads to a reduction of the bandgap on the order of 150 meV and non-trivial changes to the electron and hole mobilities. While the application of strain mostly leads to an increase in the AMR rate, we have shown that 1% tensile strain reduces the *hhe* AMR rate by 38%. Considering the combined effects of tensile strain on increasing the in-plane electron mobility[47] and suppressing the *hhe* AMR rate (i.e., increasing the lifetime of electrons in *p*-type materials), strain engineering may be a route to increase the performance of devices utilizing minority electron carriers in a *p*-type region. We note, however, that tensile strain also reduces the out-of-plane electron mobility.[47] Unfortunately, it is unlikely this approach could be directly applied to the *p*-type regions of silicon solar cells, where thicknesses on the order of 200 μm preclude the coherent application of strain. The performance of other devices such as transistors, however, which are significantly smaller, may be able to benefit by the application of tensile strain. Indeed, any application where the ideality factor ranges between 2/3 and 1 (i.e., AMR is the lifetime-limiting process) could leverage this strain engineering approach to improve efficiency.[2,8] Future studies may also investigate the non-trivial dependence of the AMR coefficients on the magnitude of strain, optimizing the interplay between the various effects for specific applications.

In summary, we apply our first-principles methodology to investigate the effects of compressive and tensile biaxial strain on Auger–Meitner recombination in silicon. The application of strain alters the electronic structure and leads to an increase in the AMR coefficient in all cases except *hhe* AMR under tensile biaxial strain, where AMR is reduced by ∼40%. We demonstrate that the effects of strain are non-trivial and give rise to qualitatively distinct behavior for the phonon-assisted AMR process. Our findings inform the application of strain to affect device performance, highlighted by increased minority carrier lifetimes in *p*-type regions.

See the supplementary material for additional information on (1) the strain effects on the phonon dispersion, (2) the quasiparticle corrections and bandgap shifts, (3) the carrier distribution changes under strain, (4) valley analysis of the electrons in the *eeh* process, (5) three-dimensional plots of the phonon contributions, and (6) distribution of excited carriers.

We thank David Young for useful discussions. This work is supported as part of the Computational Materials Sciences Program funded by the U.S. Department of Energy, Office of Science, Basic Energy Sciences under Award No. DE-SC0020129. This work used resources of the National Energy Research Scientific Computing (NERSC) Center, a DOE Office of Science User Facility supported under Contract No. DE-AC02-05CH11231. K.B. acknowledges the support of the U.S. Department of Energy, Office of Science, Office of Advanced Scientific Computing Research, Department of Energy Computational Science Graduate Fellowship under Award Number DE-SC0020347. K.B.'s editing of this manuscript was performed under the auspices of the U.S. Department of Energy by Lawrence Livermore National Laboratory under Contract No. DE-AC52-07NA27344.

AUTHOR DECLARATIONS

Conflict of Interest

The authors have no conflicts to disclose.

Author Contributions

Kyle Bushick: Conceptualization (equal); Data curation (lead); Formal analysis (lead); Investigation (lead); Methodology (equal); Software (lead); Validation (equal); Visualization (lead); Writing – original draft (lead); Writing – review & editing (equal). **Emmanouil Kioupakis:** Conceptualization (equal); Formal analysis (supporting); Funding acquisition (lead); Investigation (supporting); Methodology (equal); Project administration (lead); Resources (lead); Supervision (lead); Validation (equal); Writing – review & editing (equal).

DATA AVAILABILITY

The data that support the findings of this study are available from the corresponding author upon reasonable request.

REFERENCES

[1]D. Matsakis, A. Coster, B. Laster, and R. Sime, "A renaming proposal: "The Auger–Meitner effect"," Phys. Today **72**(9), 10–11 (2019).
[2]M. Green, "Limits on the open-circuit voltage and efficiency of silicon solar cells imposed by intrinsic Auger processes," IEEE Trans. Electron Devices **31**, 671–678 (1984).
[3]T. Tiedje, E. Yablonovitch, G. Cody, and B. Brooks, "Limiting efficiency of silicon solar cells," IEEE Trans. Electron Devices **31**, 711–716 (1984).
[4]M. J. Kerr, A. Cuevas, and P. Campbell, "Limiting efficiency of crystalline silicon solar cells due to Coulomb-enhanced Auger recombination," Prog. Photovoltaics **11**, 97–104 (2003).
[5]Q. Su, H. Lin, G. Wang, H. Tang, C. Xue, Z. Li, X. Xu, and P. Gao, "Limiting-efficiency assessment on advanced crystalline silicon solar cells with Auger ideality factor and wafer thickness modifications," Authorea (2023).
[6]M. Shibib, F. Lindholm, and J. Fossum, "Auger recombination in heavily doped shallow-emitter silicon p-n-junction solar cells, diodes, and transistors," IEEE Trans. Electron Devices **26**, 1104–1106 (1979).
[7]M. Tyagi and R. V. Overstraeten, "Minority carrier recombination in heavily-doped silicon," Solid-State Electron. **26**, 577–597 (1983).
[8]M. Leilaeioun and Z. C. Holman, "Accuracy of expressions for the fill factor of a solar cell in terms of open-circuit voltage and ideality factor," J. Appl. Phys. **120**, 123111 (2016).
[9]G. Tsutsui, S. Mochizuki, N. Loubet, S. W. Bedell, and D. K. Sadana, "Strain engineering in functional materials," AIP Adv. **9**, 030701 (2019).
[10]Z. Dai, L. Liu, and Z. Zhang, "Strain engineering of 2D materials: Issues and opportunities at the interface," Adv. Mater. **31**, 1805417 (2019).
[11]Y. Miao, Y. Zhao, S. Zhang, R. Shi, and T. Zhang, "Strain engineering: A boosting strategy for photocatalysis," Adv. Mater. **34**, 2200868 (2022).
[12]H. Omi, D. J. Bottomley, Y. Homma, and T. Ogino, "Wafer-scale strain engineering on silicon for fabrication of ultimately controlled nanostructures," Phys. Rev. B **67**, 115302 (2003).
[13]M. Ieong, B. Doris, J. Kedzierski, K. Rim, and M. Yang, "Silicon device scaling to the sub-10-nm regime," Science **306**, 2057–2060 (2004).
[14]D. J. Paul, "Si/SiGe heterostructures: From material and physics to devices and circuits," Semicond. Sci. Technol. **19**, R75–R108 (2004).
[15]P. Chidambaram, C. Bowen, S. Chakravarthi, C. Machala, and R. Wise, "Fundamentals of silicon material properties for successful exploitation of strain engineering in modern CMOS manufacturing," IEEE Trans. Electron Devices **53**, 944–964 (2006).
[16]C. Rödl, T. Sander, F. Bechstedt, J. Vidal, P. Olsson, S. Laribi, and J.-F. Guillemoles, "Wurtzite silicon as a potential absorber in photovoltaics: Tailoring the optical absorption by applying strain," Phys. Rev. B **92**, 045207 (2015).
[17]S. Meesala, Y.-I. Sohn, B. Pingault, L. Shao, H. A. Atikian, J. Holzgrafe, M. Gündoğan, C. Stavrakas, A. Sipahigil, C. Chia, R. Evans, M. J. Burek, M. Zhang, L. Wu, J. L. Pacheco, J. Abraham, E. Bielejec, M. D. Lukin, M. Atatüre, and M. Lončar, "Strain engineering of the silicon-vacancy center in diamond," Phys. Rev. B **97**, 205444 (2018).
[18]W. Cai, J. Wang, Y. He, S. Liu, Q. Xiong, Z. Liu, and Q. Zhang, "Strain-modulated photoelectric responses from a flexible α-In_2Se_3/3R MoS_2 heterojunction," Nano-Micro Lett. **13**, 74 (2021).
[19]A. M. Itsuno, J. D. Phillips, and S. Velicu, "Design of an auger-suppressed unipolar HgCdTe NBνN photodetector," J. Elec. Mater. **41**, 2886–2892 (2012).
[20]W. K. Bae, L. A. Padilha, Y.-S. Park, H. McDaniel, I. Robel, J. M. Pietryga, and V. I. Klimov, "Controlled alloying of the core–shell interface in CdSe/CdS quantum dots for suppression of Auger recombination," ACS Nano **7**, 3411–3419 (2013).
[21]J. Piprek, "Analysis of efficiency limitations in high-power InGaN/GaN laser diodes," Opt. Quant. Electron. **48**, 471 (2016).
[22]R. Singh, W. Liu, J. Lim, I. Robel, and V. I. Klimov, "Hot-electron dynamics in quantum dots manipulated by spin-exchange Auger interactions," Nat. Nanotechnol. **14**, 1035–1041 (2019).
[23]C. Livache, W. D. Kim, H. Jin, O. V. Kozlov, I. Fedin, and V. I. Klimov, "High-efficiency photoemission from magnetically doped quantum dots driven by multi-step spin-exchange Auger ionization," Nat. Photonics **16**, 433–440 (2022).
[24]S. Du, J. Yin, H. Xie, Y. Sun, T. Fang, Y. Wang, J. Li, D. Xiao, X. Yang, S. Zhang, D. Wang, W. Chen, W.-Y. Yin, and R. Zheng, "Auger scattering dynamic of photo-excited hot carriers in nano-graphite film," Appl. Phys. Lett. **121**, 181104 (2022).
[25]W. W. Lui, T. Yamanaka, Y. Yoshikuni, S. Seki, and K. Yokoyama, "Optimum strain for the suppression of Auger recombination effects in compressively strained InGaAs/InGaAsP quantum well lasers," Appl. Phys. Lett. **64**, 1475–1477 (1994).
[26]K. Bushick and E. Kioupakis, "Phonon-assisted Auger–Meitner recombination in silicon from first principles," Phys. Rev. Lett. **131**, 076902 (2023).
[27]P. Giannozzi, S. Baroni, N. Bonini, M. Calandra, R. Car, C. Cavazzoni, D. Ceresoli, G. L. Chiarotti, M. Cococcioni, I. Dabo, A. D. Corso, S. D. Gironcoli, S. Fabris, G. Fratesi, R. Gebauer, U. Gerstmann, C. Gougoussis, A. Kokalj, M. Lazzeri, L. Martin-Samos, N. Marzari, F. Mauri, R. Mazzarello, S. Paolini, A. Pasquarello, L. Paulatto, C. Sbraccia, S. Scandolo, G. Sclauzero, A. P. Seitsonen, A. Smogunov, P. Umari, and R. M. Wentzcovitch, "QUANTUM ESPRESSO: A modular and open-source software project for quantum simulations of materials," J. Phys.: Condens. Matter **21**, 395502 (2009).
[28]P. Giannozzi, O. Andreussi, T. Brumme, O. Bunau, M. B. Nardelli, M. Calandra, R. Car, C. Cavazzoni, D. Ceresoli, M. Cococcioni, N. Colonna, I. Carnimeo, A. D. Corso, S. de Gironcoli, P. Delugas, R. A. DiStasio, A. Ferretti, A. Floris, G. Fratesi, G. Fugallo, R. Gebauer, U. Gerstmann, F. Giustino, T. Gorni, J. Jia, M. Kawamura, H.-Y. Ko, A. Kokalj, E. Küçükbenli, M. Lazzeri, M. Marsili, N. Marzari, F. Mauri, N. L. Nguyen, H.-V. Nguyen, A. O. de-la Roza, L. Paulatto, S. Poncé, D. Rocca, R. Sabatini, B. Santra, M. Schlipf, A. P.

Seitsonen, A. Smogunov, I. Timrov, T. Thonhauser, P. Umari, N. Vast, X. Wu, and S. Baroni, "Advanced capabilities for materials modelling with QUANTUM ESPRESSO," J. Phys.: Condens. Matter **29**, 465901 (2017).
[29]P. Giannozzi, O. Baseggio, P. Bonfà, D. Brunato, R. Car, I. Carnimeo, C. Cavazzoni, S. de Gironcoli, P. Delugas, F. F. Ruffino, A. Ferretti, N. Marzari, I. Timrov, A. Urru, and S. Baroni, "QUANTUM ESPRESSO toward the exascale," J. Chem. Phys. **152**, 154105 (2020).
[30]D. M. Ceperley and B. J. Alder, "Ground state of the electron gas by a stochastic method," Phys. Rev. Lett. **45**, 566–569 (1980).
[31]J. P. Perdew and A. Zunger, "Self-interaction correction to density-functional approximations for many-electron systems," Phys. Rev. B **23**, 5048–5079 (1981).
[32]N. Troullier and J. L. Martins, "Efficient pseudopotentials for plane-wave calculations," Phys. Rev. B **43**, 1993–2006 (1991).
[33]G. Bona and F. Meier, "Observation of the spin-orbit splitting at the valence band edge of silicon by spin-polarized photoemission," Solid State Commun. **55**, 851–855 (1985).
[34]S. Poncé, F. Macheda, E. R. Margine, N. Marzari, N. Bonini, and F. Giustino, "First-principles predictions of Hall and drift mobilities in semiconductors," Phys. Rev. Res. **3**, 043022 (2021).
[35]M. Zacharias, M. Scheffler, and C. Carbogno, "Fully anharmonic nonperturbative theory of vibronically renormalized electronic band structures," Phys. Rev. B **102**, 045126 (2020).
[36]N. Marzari, A. A. Mostofi, J. R. Yates, I. Souza, and D. Vanderbilt, "Maximally localized Wannier functions: Theory and applications," Rev. Mod. Phys. **84**, 1419–1475 (2012).
[37]G. Pizzi, V. Vitale, R. Arita, S. Blügel, F. Freimuth, G. Géranton, M. Gibertini, D. Gresch, C. Johnson, T. Koretsune, J. Ibañez-Azpiroz, H. Lee, J.-M. Lihm, D. Marchand, A. Marrazzo, Y. Mokrousov, J. I. Mustafa, Y. Nohara, Y. Nomura, L. Paulatto, S. Poncé, T. Ponweiser, J. Qiao, F. Thöle, S. S. Tsirkin, M. Wierzbowska, N. Marzari, D. Vanderbilt, I. Souza, A. A. Mostofi, and J. R. Yates, "Wannier90 as a community code: New features and applications," J. Phys.: Condens. Matter **32**, 165902 (2020).
[38]W. Bludau, A. Onton, and W. Heinke, "Temperature dependence of the band gap of silicon," J. Appl. Phys. **45**, 1846–1848 (1974).
[39]J. Munguía, G. Bremond, J. M. Bluet, J. M. Hartmann, and M. Mermoux, "Strain dependence of indirect band gap for strained silicon on insulator wafers," Appl. Phys. Lett. **93**, 102101 (2008).
[40]A. Richter, S. W. Glunz, F. Werner, J. Schmidt, and A. Cuevas, "Improved quantitative description of Auger recombination in crystalline silicon," Phys. Rev. B **86**, 165202 (2012).
[41]E. Kioupakis, D. Steiauf, P. Rinke, K. T. Delaney, and C. G. V. D. Walle, "First-principles calculations of indirect Auger recombination in nitride semiconductors," Phys. Rev. B **92**, 035207 (2015).
[42]J. Dziewior and W. Schmid, "Auger coefficients for highly doped and highly excited silicon," Appl. Phys. Lett. **31**, 346–348 (1977).
[43]R. Häcker and A. Hangleiter, "Intrinsic upper limits of the carrier lifetime in silicon," J. Appl. Phys. **75**, 7570–7572 (1994).
[44]M. Govoni, I. Marri, and S. Ossicini, "Auger recombination in Si and GaAs semiconductors: *Ab initio* results," Phys. Rev. B **84**, 075215 (2011).
[45]S. Dominici, H. Wen, F. Bertazzi, M. Goano, and E. Bellotti, "Numerical evaluation of Auger recombination coefficients in relaxed and strained germanium," Appl. Phys. Lett. **108**, 211103 (2016).
[46]S. Sze and K. K. Ng, *Physics of Semiconductor Devices* (John Wiley & Sons, Inc., 2006).
[47]D. Yu, Y. Zhang, and F. Liu, "First-principles study of electronic properties of biaxially strained silicon: Effects on charge carrier mobility," Phys. Rev. B **78**, 245204 (2008).